Higher trends but larger uncertainty and geographic variability in 21st century temperature and heat waves

Auroop R. Ganguly[a,1], Karsten Steinhaeuser[a,b], David J. Erickson III[c], Marcia Branstetter[c], Esther S. Parish[a], Nagendra Singh[a], John B. Drake[c], and Lawrence Buja[d]

[a]Geographic Information Science and Technology Group, Computational Sciences and Engineering Division, Oak Ridge National Laboratory, Oak Ridge, TN 37831; [b]Department of Computer Science and Engineering, University of Notre Dame, Notre Dame, IN 46556; [c]Computational Earth Sciences Group, Computer Science and Mathematics Division, Oak Ridge National Laboratory, Oak Ridge, TN 37831; and [d]National Center for Atmospheric Research, Boulder, CO 80305

Edited by Stephen H. Schneider, Stanford University, Stanford, CA, and approved July 31, 2009 (received for review April 23, 2009)

Generating credible climate change and extremes projections remains a high-priority challenge, especially since recent observed emissions are above the worst-case scenario. Bias and uncertainty analyses of ensemble simulations from a global earth systems model show increased warming and more intense heat waves combined with greater uncertainty and large regional variability in the 21st century. Global warming trends are statistically validated across ensembles and investigated at regional scales. Observed heat wave intensities in the current decade are larger than worst-case projections. Model projections are relatively insensitive to initial conditions, while uncertainty bounds obtained by comparison with recent observations are wider than ensemble ranges. Increased trends in temperature and heat waves, concurrent with larger uncertainty and variability, suggest greater urgency and complexity of adaptation or mitigation decisions.

climate change | extremes | regional analysis

Recent observations of global-average emissions (1, 2) show higher trajectories than the worst-case A1FI scenario reported in IPCC AR4 (3). Average A1FI temperatures (1, 4) trend higher than the best-case B1 as well as the relatively worse-case A2 scenario (5). Model simulations, validated with observations, have pointed to more intense, longer lasting, and more frequent heat waves in the 21st century (6). However, a rigorous statistical validation of the increased global warming and heat waves, followed by an investigation of the trends at regional scales, is required for decision-makers and end-users. Larger trends in warming and extremes suggest a greater urgency to develop adaptation and mitigation strategies (7, 8). On the other hand, a comprehensive assessment of the uncertainties and geographical variability provide an understanding of the tradeoff space for risk-informed decisions (9), which refers to different tactical or strategic options that may be available to a decision-maker for climate change adaptation and mitigation. Uncertainty of climate model projections has been quantified (10-14) either by comparing model hindcasts with observations or by comparing an ensemble of simulations. However, hindcasts validate models after the fact and hence risk underestimating predictive ability (15), while ensembles may only capture specific aspects of the variability. Hence the reliable and timely analysis of evolving climate model projections, extremes, and uncertainty remains a challenge (16-21).

Results

Statistically Higher Warming Trends. First, we show that the global-average temperatures from the middle to end of the 21st century are likely to be higher than previously believed (3). This is suggested by the fact that recent observed emissions trend toward or above A1FI assumptions (1, 2). The fact that observed emissions are at or above the level of A1FI, or any given scenario, in the current decade may not be a compelling reason to support conclusions about temperature in the late 21st century, as the trends could change considerably. However, when recent observations match or exceed the higher end of the emissions scenarios, then the latter cannot be ruled out as an implausible scenario. Moreover, we are not aware of any studies that clearly show that the higher temperature trends based on A1FI are statistically significant compared to other scenarios like A2 or B1. Here, A1FI simulations from CCSM 3.0 (22) are being evaluated. The assumptions inherent in the design of the A1FI and the A2 scenarios cause the A1FI emissions trajectories to be higher than A2 in the latter half of the 21st century; but while A2 continues to increase thereafter, A1FI begins to stabilize. The two scenarios converge toward the end of the century because of competing factors. Specifically, the A1FI envisions a more fossil-fuel intensive situation but also a more convergent world as compared to A2 (see reference 5 for details).

We performed a *t*-test ($\alpha = 0.05$) to determine if the mean A1FI outputs are higher than the mean A2 and B1 outputs at significant levels. Fig. 1 shows the global-average temperature projections, along with confidence bounds (three standard deviations on either side) at each decade. Our results (details in SI) show that both A1FI and A2 temperature projections are statistically distinguishable from the B1 scenario from 2040–2100 at 95% confidence; A1FI projections are statistically distinguishable from A2 from 2060–2090, but become indistinguishable again in 2100. During 2000–2007, when comparisons with observations are made, and until 2030, the B1, A2, and A1FI scenarios are statistically indistinguishable at 95% confidence. These statistical significance tests rely on important assumptions and uncertainty estimates (SI). The bottom-right panel of Fig. 1 shows monthly global-average temperatures (the "seasonality" in this case is caused by the distribution of land surfaces in the northern versus the southern hemispheres); visually, there is a clear match with reanalysis and observations, as well as an increasing trend in 2050 and 2100.

Significant Geographic Variability. Global averages are important (21), but a complete picture of projected trends and uncertainty emerges only when the results are analyzed geographically. Furthermore, stakeholders and end-users require credible as-

ENVIRONMENTAL SCIENCES

Author contributions: A.R.G. designed research; A.R.G. and K.S. performed research; D.J.E., M.B., J.B.D., and L.B. contributed new reagents/analytic tools; K.S., E.S.P., and N.S. analyzed data; and A.R.G., K.S., and D.J.E. wrote the paper.

The authors declare no conflicts of interest.

This article is a PNAS Direct Submission.

Freely available online through the PNAS open access option.

[1]To whom correspondence should be addressed. E-mail: gangulyar@ornl.gov.

This article contains supporting information online at www.pnas.org/cgi/content/full/0904495106/DCSupplemental.

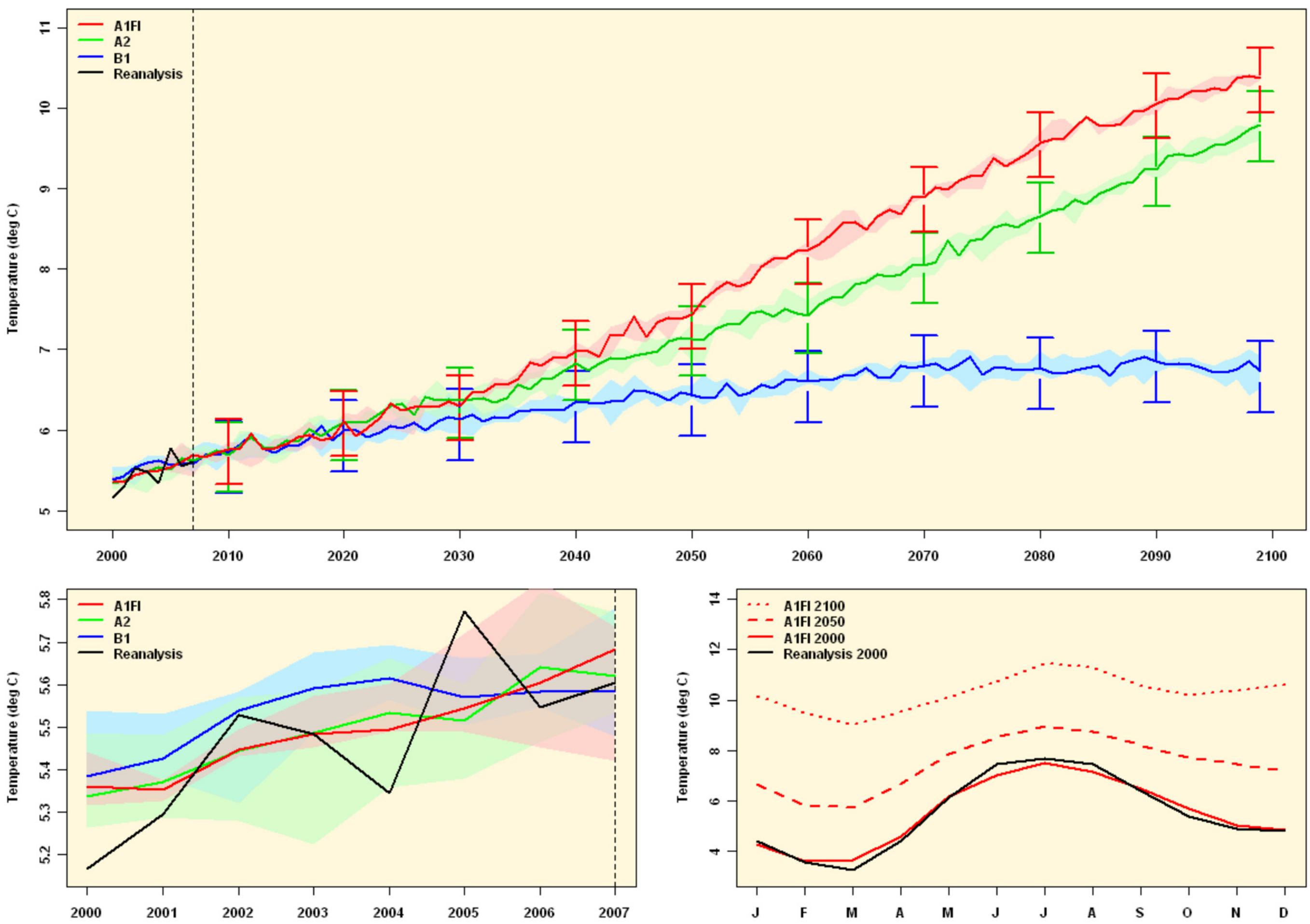

Fig. 1. Global average projections of temperatures and uncertainty. The top panel shows globally-average temperature (°C) projections from CCSM 3.0, based on A1FI, A2, and B1, along with error bars. The bias and standard deviations are calculated for each projection by comparing NCEP Reanalysis data with model outputs in 2000–2007, which forms the basis in the generation of the error bars for 2010 to 2100; note that the error bars are based solely on this bias and variance, but do not take into account the effect of projection lead times. The shaded areas indicate uncertainties caused by five initial-condition ensembles. The bottom left panel zooms in on 2000–2007. The bottom right panel shows monthly global-average temperatures.

sessments of climate change and extremes at local to regional scales for adaptation decisions and policy negotiations (7, 8). Here we compare A1FI-driven CCSM 3.0 (22) model projections and NCEP Reanalysis (23) observations for 2000–2007, when both are available, and develop grid-based estimates for model bias and standard deviation. We use the results to generate bias-corrected "most likely" projections and corresponding confidence bounds based on three standard deviations at each grid cell. Grid-based decadal averages are calculated for three time periods: The current "2000" decade, the mid-century "2050" decade, and the end-century "2100." The "2050" and "2100" values are subtracted from the "2000" values to show the change. A1FI temperatures start to significantly depart from B1 and A2 scenarios around 2050 and reconverge with A2 around 2100 (Fig. 1). The variables plotted in Figs. 2 and 3 are based on decadal average temperatures and Fig. 4 on a measure of the intensity of heat waves (6), all in degrees Celsius. While the maps have global coverage, the precision of the numbers are the same as CCSM 3.0 model outputs (1.4° × 1.4° grid), so the results can be used for regional analysis; visualizations were interpolated with commercial GIS software.

Decadal average temperatures from the model and observations, as well as the bias (details in SI), are shown in top panel of Fig. 2. While model and observations appear visually similar in 2000–2007, the geographical variability is significant. Temperatures over land appear to be mostly overpredicted (especially at high altitudes), with exceptions in higher latitudes, where the biases are low, and in desert areas, where there is some underprediction. Oceans are well-predicted due to thermal inertial effects, except for parts of the Atlantic around the current ice-edges that are underpredicted. The bottom two panels show temperature differences in 2050 and 2100 compared to 2000. The most likely temperature increases in 2050 are high almost all over the globe; however, the disparity between the upper and lower bounds is significant. The 2050 upper bound map looks similar to the 2100 most likely map, while the 2050 lower bound map is covered globally with small negative values. The geographic variability is large with relatively distinct regional patterns. The upper and lower bound maps in 2050, therefore, present two contrasting pictures of the globe. The 2100 maps show significant overall warming, even at the lower bound, while the upper bounds for both 2050 and 2100 show an increasingly grim state of the world. This is a unique method of examining trends in global climate prediction.

The geographical variability of temperature differences from the A1FI-based projections in 2000, 2050, and 2100 are compared with those from B1 and A2 in Fig. 3. Projections from the three scenarios are indistinguishable even at small significance levels in 2000, although A1FI appears slightly lower than both B1 and A2 over large portions of the globe. In 2050 and 2100, A1FI

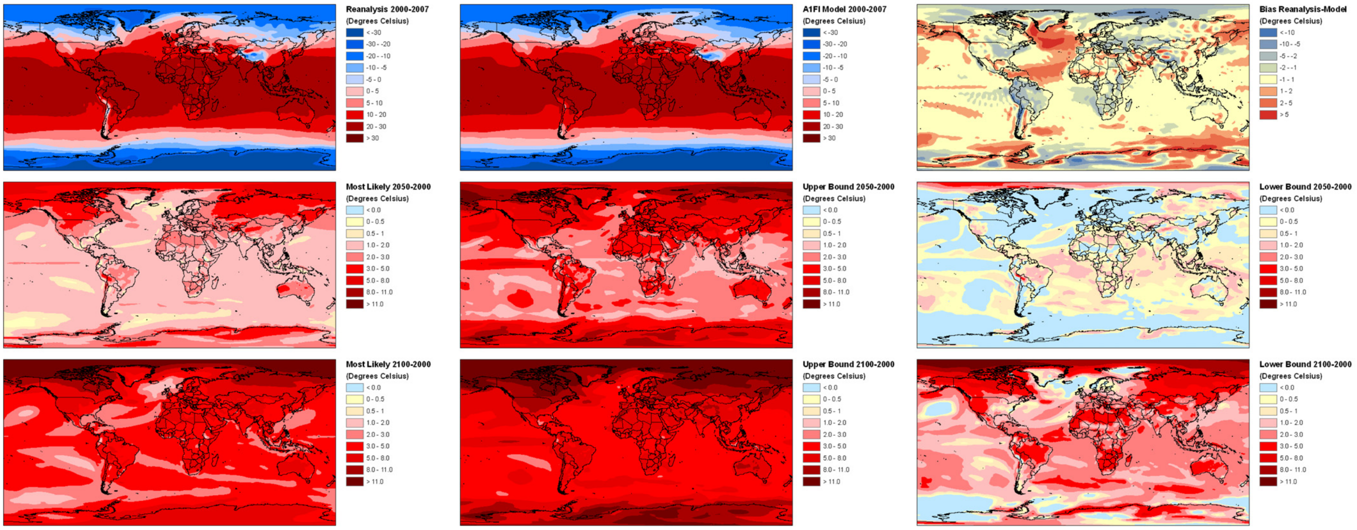

Fig. 2. Grid-based temperature projections with confidence bounds for A1FI. The top panel shows reanalysis and model-simulated annual average temperature (°C) along with the bias for 2000–2007. The bottom panels show 2050 and 2100 temperature projections from A1FI-forced CCSM 3.0 after bias correction (most likely maps, left) as well as upper (center) and lower (right) bounds. The numbers can be used to support local to regional scale analyses of climate change and extreme hydrometeorological stresses or impacts.

projections are much higher than B1 for almost all grid cells. The difference between the A1FI and A2 in 2050 is not statistically significant on average, but we find significant variability in scattered regions across the map. However, by 2100, A1FI is visually much higher than A2, especially in the northern hemisphere. To emphasize the uncertainty stemming from the geographic variability of the model, we also perform a comparison between individual ensemble members of the A1FI scenario (see SI).

Increasing Intensity-Duration-Frequency of Heat Waves. The intensity of heat waves across the world at CCSM 3.0 resolutions are investigated in Fig. 4. A heat wave here is defined as the mean annual 3-day warmest nighttime minima event, following previous researchers (6). The top two panels show that, while the model-generated and observed severity of heat waves in 2000–2007 exhibit similar patterns, there is a distinct bias. The observed heat wave intensity is consistently higher than A1FI projections in the current decade when global averages are considered. However, the large geographic variability of the observed and modeled heat wave intensities, as well as the significant uncertainties and geographic variability of the model biases, imply that this may not necessarily be true for all regions. Heat waves over land masses are nearly all overpredicted, with exception of the higher latitudes and certain desert regions, while the oceans are better predicted except in the Atlantic, where they are underpredicted. The two bottom panels show the projections for 2050 and 2100. Increased severity of heat waves is observed in nearly all of the land masses around the globe (except at high latitudes), as well as most of the low- to mid-latitude oceanic regions. The increases in heat wave intensity do not necessarily follow the warming patterns. Thus, the Western part of the United States show larger temperature increase, but the heat waves appear to be concentrated in the Midwest and Southeast. This clear difference in the geographical distribution of heat waves and simple warming is a critical point of this communication. We also investigate the duration and frequency of heat waves (see SI).

Discussion

We analyze NCEP Reanalysis observations and climate model simulations, including developed A1FI-forced ensembles generated from the CCSM 3.0 model, to develop bias-corrected

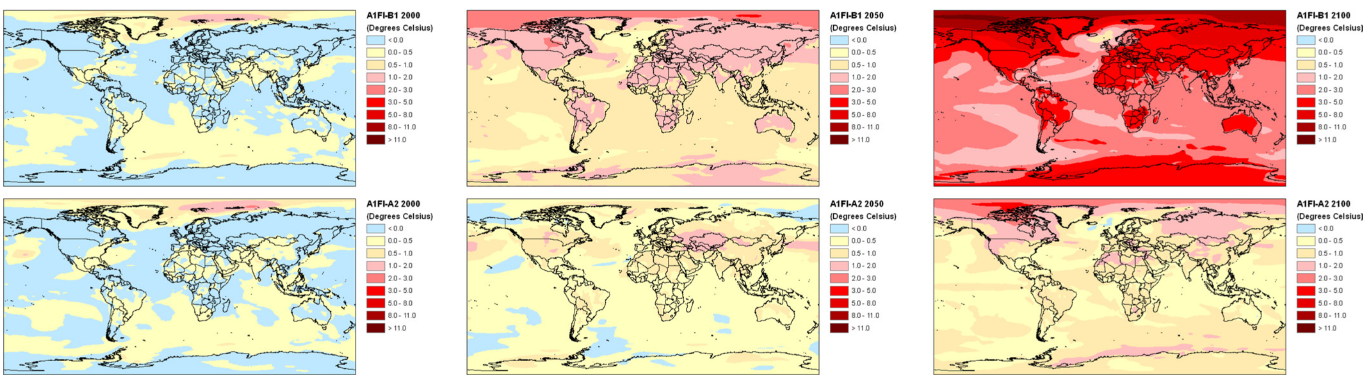

Fig. 3. Comparing grid-based A1FI projections with A2 and B1. Temperatures generated for the A1FI scenario in 2000, 2050, and 2100 are subtracted from the other scenarios: The figures on the left show 2000, during which time the scenarios are not separated. The figures on the right for 2050 and 2100 show the difference of A1FI with B1 (top) and A2 (bottom).

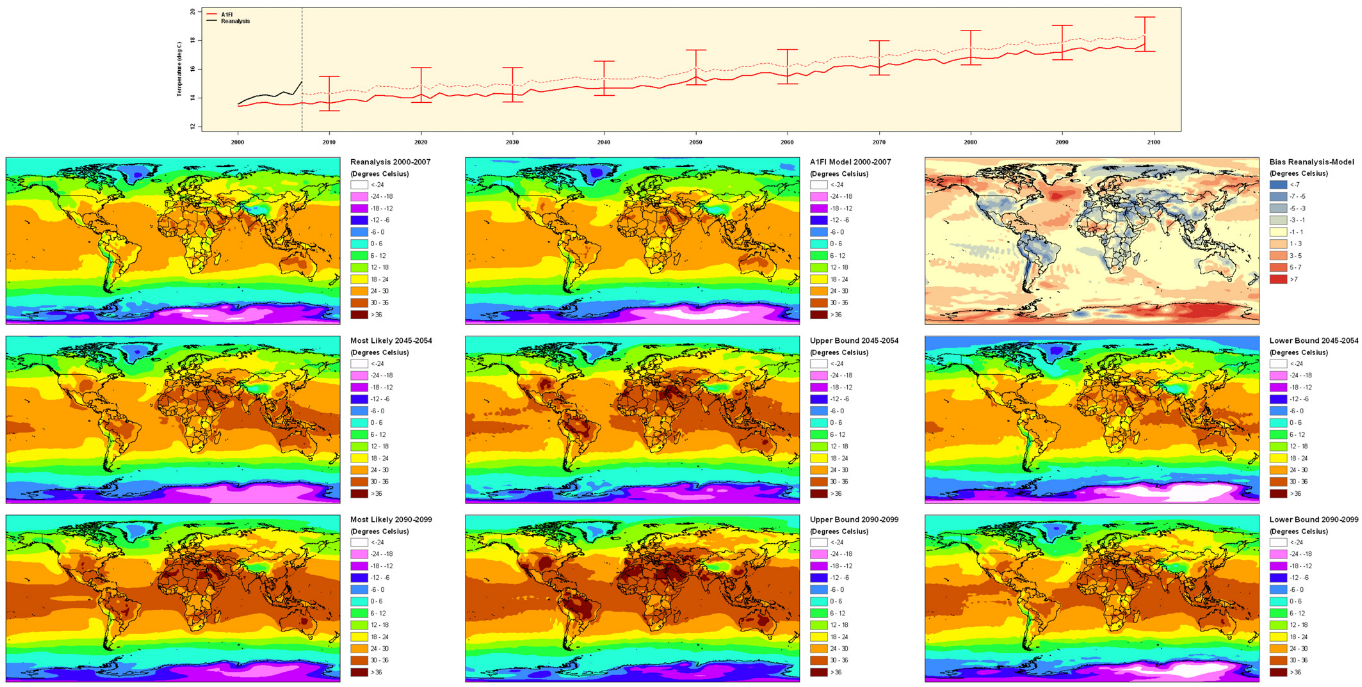

Fig. 4. Intensity of heat waves from A1FI. A heat wave is defined as the mean annual consecutive 3-day warmest nighttime minima event. The top two panels show intensity, graphically and mapped, from reanalysis data and model outputs for 2000–2007 along with the bias. The bottom panels show 2050 and 2100 heat wave projections from A1FI-forced CCSM 3.0 after bias correction (most likely maps, left) as well as upper (center) and lower (right) bounds. The numbers can be used to support local to regional scale analyses of climate change and extreme hydrometeorological stresses or impacts.

projections as well as uncertainty bounds for decadal-averages of temperature and heat waves. The uncertainty bounds are based on the differences between the model-simulations and observations, which are shown to follow a relatively stationary Gaussian distribution. The confidence bounds based on three standard deviations are consistently greater than the maximum ensemble ranges. In addition, these bounds can be larger than the differences between scenarios. Thus, the projected global-average temperatures from the different SRES scenarios cannot be statistically distinguished from each other at 95% confidence levels until about 2030, and the two more extreme scenarios (A2 and A1FI) cannot be distinguished from each other until the middle of the 21st century. This remains true even though the temperature changes are clearly distinguishable when compared across multiple decades for any one given scenario. However, the trends in A1FI-forced global-averaged temperatures are significantly higher from 2050 onwards, until they converge back with A2 toward the end of the century following the emissions trajectories. We note that the IPCC SRES scenarios are a suite of baseline nonpolicy scenarios that are not intended to span the full range of possible future emissions. A worst-case scenario could have higher emissions than A1FI, and a scenario including climate policy could have lower emissions than B1. A strict interpretation would identify A1FI as the "highest" scenario reported in IPCC AR4 and B1 as the "lowest," which is a relative labeling. Our use of the terms "worst case" and "best case," which borrowed from labeling (e.g., 24), may need to be interpreted accordingly. An examination of the regional variability based on daily data at 1.4° Gaussian grids reveals that the uncertainty bounds are large enough to make the warming appear insignificant on the lower bounds until 2050, but very significant at regional scales. Larger upper bounds imply that decision-makers need to be prepared for the worst possible consequences even though the most likely and lower bounds provide a way to optimize the allocation of potentially limited resources to manage the adverse effects. An investigation of decadal-average heat wave intensities at regional scales similarly reveals a large bias and uncertainty bounds. The globally averaged intensity of heat waves at decadal scales shows that the observed intensities are higher than the worst-case model projections in the current decade, which implies further exacerbation of heat waves compared to what has been already suggested by previous researchers. Future research needs to further validate the insights developed here through multimodel ensembles. The insights about trends in temperatures and heat waves, as a function of emissions trajectories, are expected to remain unaltered. However, the use of multiple models will likely increase the uncertainties and variability at both global and regional scales.

Materials and Methods

From the CCSM 3.0 model, we obtained five-member ensembles for IPCC SRES A2 and B1 and three runs for A1FI. We consider the ensemble median for visualization where applicable. The model data were provided at T85 resolution (approximately 1.4° × 1.4° grid) and NCEP/NCAR Reanalysis data at T62 resolution (approximately 2.5° × 2.5° grid). We use a bivariate spline (25) to interpolate the model data onto the reanalysis grid. Bias was computed for the 8-year period from 2000–2007, due to the need for both model and reanalysis data. The remainder of our analyses use three decades at the beginning, middle, and end of the 21st century: 2000–2009, 2045–2054, and 2090–2099; in our figures these are labeled as 2000, 2050, and 2100, respectively. All figures show decadal averages over each of these periods, in plots as global average and in maps computed individually at each grid location. For temperature extremes, we adopt a definition of heat waves that focuses on intensity of the event (6).

All statistics are performed using the software environment R (www.r-project.org) and the package akima (R package version 0.5–1; http://cran.r-project.org/web/packages). Maps were produced using commercial GIS software ArcGIS 9.3 (www.esri.com/software/arcgis).

ACKNOWLEDGMENTS. We thank Dr. Shih-Chieh Kao of Oak Ridge National Laboratory (ORNL) for his comments. This research was supported by the Laboratory-Directed Research and Development Program of the Oak Ridge National Laboratory, managed by UT Battelle, LLC, for the U.S. Department of Energy under Contract DE-AC05-00OR22725.

1. Raupach MR, et al. (2007) Global and regional drivers of accelerating CO_2 emissions. *Proc Natl Acad Sci USA* 104:10288–10293.
2. Marland G (2008) Uncertainties in accounting for CO_2 from fossil fuels. *J Ind Ecol* 12:136–139.
3. IPCC (2007) *Fourth Assessment Report: Climate Change 2007* (Cambridge University Press, Cambridge, UK).
4. Hadley Centre (2003) *Climate Change: Observations and Predictions* (Met Office, Exeter, UK).
5. Nakicenovic N, Swart R, Eds (2000) *Special Report on Emissions Scenarios* (Cambridge University Press, Cambridge, UK).
6. Meehl G, Tebaldi C (2004) More intense, more frequent, and longer lasting heat waves in the 21st century. *Science* 305:994–997.
7. Stainforth DA, Allen MR, Tredger ER, Smith LA (2007) Confidence, uncertainty and decision-support relevance in climate predictions. *Philos Trans R Soc London Ser A* 365:2145–2161.
8. Stainforth DA, Downing TE, Washington R, Lopez A (2007) Issues in the interpretation of climate model ensembles to inform decisions. *Philos Trans R Soc London Ser A* 365:2163–2177.
9. Dessai S, O'Brien K, Hulme M (2007) Editorial: On uncertainty and climate change. *Global Environ Change* 17:1–3.
10. Lopez A, et al. (2006) Two approaches to quantifying uncertainty in global temperature changes. *J Clim* 19:4785–4796.
11. Barnett DN, Brown SJ, Murphy JM, Sexton DMH, Webb MJ (2006) Quantifying uncertainty in changes in extreme event frequency in response do doubled CO_2 using a large ensemble of GCM simulations. *Clim Dyn* 26:489–511.
12. Tebaldi C, Smith RL, Nychka D, Mearns LO (2005) Quantifying uncertainty in projections of regional climate change: A Bayesian approach to the analysis of multimodel ensebles. *J Clim* 18:1524–1540.
13. Stott PA, Forest CE (2007) Ensemble climate predictions using climate models and observational constraints. *Philos Trans R Soc London Ser A* 365:2029–2052.
14. Toth Z, Kalnay E (1997) Ensemble forecasting at NCEP and the breeding method. *Mon Weather Rev* 125:3297–3319.
15. Stainforth D, et al. (2005) Uncertainty in predictions of climate response to rising levels of greenhouse gases. *Nature* 433:403–406.
16. Stott PA, Kettleborough JA (2002) Origins and estimates of uncertainty in predictions of twenty-first century temperature rise. *Nature* 416:723–726.
17. Collins M, et al. (2006) Towards quantifying uncertainty in transient climate change. *Clim Dyn* 27:127–147.
18. Pielke RA (2008) Overheated claims. *Financial Post*, June 17.
19. Rahmstorf S (2007) Recent climate observations compared to projections. *Science* 316:709.
20. Berliner ML, Kim Y (2008) Bayesian design and analysis for superensemble-based climate forecasting. *J Clim* 21:1891–1910.
21. Watson J (2008) Certainty and uncertainty in climate change predictions: What use are climate models? *Environ Resour Econ* 39:37–44.
22. Drake JB, Jones PW, Carr GR (2005) Overview of the software design of the community climate system model. *Int J High Perform C* 19:177–186.
23. Kistler R, et al. (2001) The NCEP-NCAR 50 year reanalysis. *Bull Am Meteorol Soc* 82:247–268.
24. Tollefson J (2008) Climate war games. *Nature* 454:673.
25. Hiroshi A(1978) A method of bivariate interpolation and smooth surface fitting for irregularly distributed data points. *ACM Trans Math Software* 4:148–159.